Numerical Research on Interfacial Damage and Sealing Reliability of Flexible Joint under Wide Temperature Range *

SHI Hong-bin，WANG Cai，QU Zhuan-li，LI Guo-cai

（Science and Technology on Combustion，Internal Flow and Thermo-Structure Laboratory，
Xi'an Aerospace Solid Propulsion Technology Institute，Xi'an 710025，China）

Abstract：Interfacial failure is a serious problem in the solid rocket motor flexible joint. In order to investigate the damage rules of bonding interfaces during flexible joint swinging under wide temperature range（-55℃～65℃）, a three-dimensional non-linear finite element analysis was established based on ABAQUS 6.14. Cohesive zone model was adopted as the constitutive model of adhesive to obtain the damage parameters. Additionally, combined with the interfacial contact stress, one computational method to calculate the sealing reliability of flexible joint was proposed. Results illustrate that the mechanical behavior of adhesive and butyl isoprene rubber both decrease gradually with the increase of temperature, indicating that fracture occurs easily at a high temperature. The correspondence relationship between sealing reliability and interfacial damage is confirmed to be inversely related. The damage of flexible joint increases gradually first and grows rapidly above -40℃ with temperature raising, while the sealing reliability presents a linear downward trend first and then slows down above 20℃ with temperature. The sealing reliability reaches maximum at -55℃ under wide temperature range.

Key words：Flexible joint；Interfacial damage；Cohesive zone model；Sealing reliability；Wide temperature range

CLC number：V435.3　**Document code**：A　**Article number**：1001-4055（2019）10-2313-12

DOI：10.13675/j.cnki. tjjs. 190136

宽温域下柔性接头界面损伤及密封可靠性数值研究 *

史宏斌，王　才，屈转利，李国才

（西安航天动力技术研究所，燃烧、热结构和内流场重点实验室，陕西 西安 710025）

摘　要：界面失效是固体火箭发动机柔性接头的重要问题。为研究宽温域（-55℃～65℃）下柔性接头摆动过程中界面的损伤规律，基于ABAQUS 6.14建立了柔性接头的三维非线性有限元分析模型，并采用内聚力模型作为粘接界面的本构模型，获得了界面的损伤参数。此外，结合界面间的接触应力，提出了一种计算柔性接头密封可靠度的方法。结果表明，宽温域下粘接界面与丁异戊橡胶的力学性能随温度的升高而逐渐下降，说明柔性接头在高温段更容易发生失效；并且确认了柔性接头密封可靠度与界面损伤间成反比关系，宽温域下随着温度升高，柔性接头损伤程度先缓慢增大，-40℃后出现迅速增加，而柔性接头密封可靠度先呈线性下降趋势，20℃后下降趋势放缓，-55℃时柔性接头密封可靠度最大。

关键词：柔性接头；界面损伤；内聚力模型；密封可靠性；宽温域

---

* **收稿日期**：2019-03-02；**修订日期**：2019-06-02。

通讯作者：史宏斌，男，博士，研究员，研究领域为固体火箭发动机柔性喷管。E-mail: shihongbin8171@163.com

引用格式：史宏斌，王　才，屈转利，等. 宽温域下柔性接头界面损伤及密封可靠性数值研究[J]. 推进技术，2019，40(10)：2313-2324. （SHI Hong-bin，WANG Cai，QU Zhuan-li，et al. Numerical Research on Interfacial Damage and Sealing Reliability of Flexible Joint under Wide Temperature Range[J]. *Journal of Propulsion Technology*，2019，40（10）：2313-2324.）

1 Introduction

Flexible joint, composed of spherical elastomers alternating with metal or composite material reinforcements (see Fig. 1(a)), is the most important component to achieve thrust vector control (TVC) in solid rocket motor[1-3]. Due to the advantage of full-axis swing, large lateral force, small thrust loss as well as excellent vectoring repeatability, the flexible joint is widely used in large strategic motors, boosters (see Fig. 1 (b)) as well as miniature tactical missiles[4-8]. According to the structure of flexible joint, the performance is decided by the interfacial reliability. Recently, interfacial debonding between elastomer and reinforcement has appeared in the ground tests of solid rocket motors. Interfacial failure is mostly happened after several times swing due to stress concentration, which is caused by residual stress coupled with vectoring stress. At present, most missiles are demanded the capability of all-weather combat to adapt plateaus、deserts and oceans, meaning that the flexible joint need to keep excellent sealing reliability under wide temperature range from −55℃ to 65℃.

The finite element method is commonly used in flexible joint simulation owing to the difficulty of retrieving interfacial parameters by tests. Usually, obtaining stress/strain distribution of elastomer as well as the influence on spring ratio torque is the focus in simulation[9-13]. In these cases, tie constraint is adopted between elastomer and reinforcement but can't get interfacial damage. The investigation about interfacial damage of flexible joint is few, An[14] found that large axial stress is the main reason of interfacial damage by analyzing interfacial axis stress and shear stress. However, the constitutive model of interface was not put forward and no quantitative description was used. Wang[15] calculated the safety factor of the elastomer in order to reflect the reliability of flexible joint by adopting normal and tangential stress. This method also hasn't proposed constitutive model of adhesive and can only reflect the design margin of flexible joint, and the interfacial damage hasn't been evaluated. The interfacial mechanical properties vary differently, and the damage as well as reliability are distinct under wide temperature range[16-18]. Based on the above, the previous research is insufficient to evaluate the reliability of flexible joint.

To investigate the interfacial damage and sealing reliability of flexible joint, this paper adopts cohesive zone model[19-21] instead of tie constraint between elastomer and reinforcement according to the structural and working characteristics of flexible joint. The damage parameters are acquired by simulation in order to define the damage of interfaces and flexible joint. Also, the contact stress is extracted to calculate the sealing reliability of flexible joint. In this way, the reliability of flexible joint is evaluated accurately and significant guidance is provided in structural design and material selection under wide temperature range.

2 Calculation model

2.1 Cohesive zone model

2.1.1 Theory of cohesive zone model

The cohesive zone model, proposed by Dugdale D S and Barenblatt G I[22-23], is widely used in the simula-

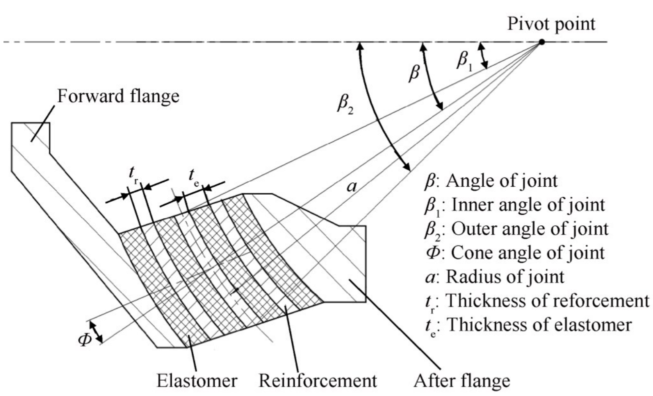

(a) Structure of flexible joint

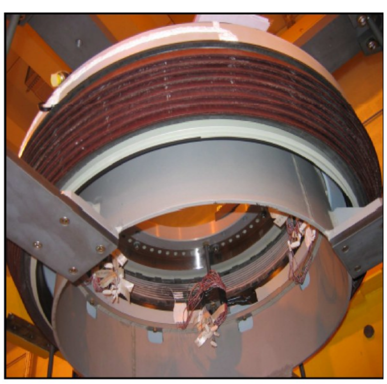
(b) Flexible joint of Vega I: P80 motor[8]

Fig. 1 Flexible joint

tion of interfacial damage. There are three propagation modes of cracks called Mode-I, Mode-II and Mode-III. Using cohesive zone model will acquire the initial location as well as position and shape of crack tip, most importantly, singularity of stress has been eliminated. Fig. 2 shows the bilinear traction-separation characteristics which has been adopted to simulate bondline in this paper. The interface is in a linear elastic state before damage initiation and the damage will be produced when the separation displacement reaches δ_0, and the element will invalid when reaches δ_{max}. The area surrounded by curves is the maximum energy release rate that G_{IC}, G_{IIC}, G_{IIIC} are corresponding to mode I, II, III cracks.

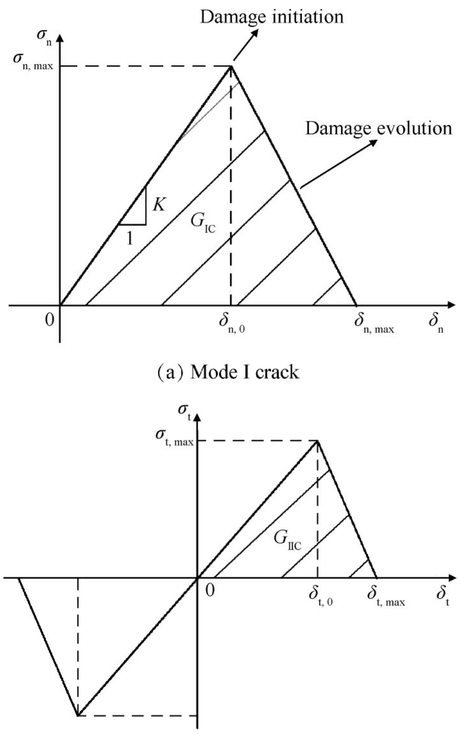

(a) Mode I crack

(b) Mode II crack

Fig. 2 Bilinear traction separation law

Quadratic traction damage initiation criterion, as follows, was used in simulation. σ represents stress and the subscript n, t, c mean three directions in space: normal, tangential and circumferential.

$$\left\{\frac{\langle\sigma_n\rangle}{\sigma_{n,max}}\right\}^2+\left\{\frac{\sigma_t}{\sigma_{t,max}}\right\}^2+\left\{\frac{\sigma_c}{\sigma_{c,max}}\right\}^2\geqslant 1 \tag{1}$$

where<>is Macauley operator defined as

$$\langle a\rangle=\begin{cases}a, & a>0\\ 0, & a<0\end{cases} \tag{2}$$

Representing that there is no damage when interface is in compression.

Benzeggagh-Kenane law[24] was implemented as the mixed mode of damage evolution because crack propagation mode is consisted of more than one fundamental mode actually and adopting single damage evolution law will lead to large deviation[25-26]. Equivalent separation displacement δ_m of mixed mode can be expressed as

$$\delta_m=\sqrt{<\delta_n>^2+\delta_t^2+\delta_c^2} \tag{3}$$

Therefore, the damage initiation separation displacement and the fracture separation displacement of mixed mode can be described as follows respectively.

$$\delta_{m,0}=\begin{cases}\sqrt{(\delta_{n,0})^2+\delta_t^2+\delta_c^2}, & \delta_n=\delta_{n,0}\\ \sqrt{\delta_n^{\ 2}+(\delta_{i,0})^2+\delta_j^2}, & \delta_i=\delta_{i,0}\,(i,j=\mathrm{t,c};\ i\neq j)\end{cases} \tag{4}$$

$$\delta_{m,f}=\begin{cases}\dfrac{2}{K\delta_{m,0}}\left[G_{IC}+\left(G_{IIC}-G_{IC}\right)\left(\dfrac{\beta^2}{1+\beta^2}\right)^{\eta}\right] & \delta_n>0\\ \sqrt{(\delta_{t,f})^2+(\delta_{c,f})^2} & \delta_n\leqslant 0\end{cases} \tag{5}$$

Where K is stiffness, $\beta^2=(\delta_t^2+\delta_c^{\ 2})/\delta_n^{\ 2}$ represents hybridization of propagation modes and η is Benzeggagh-Kenane coefficient.

The damage parameter D is defined as

$$D=\frac{\delta_{m,f}(\delta_{m,max}-\delta_{m,0})}{\delta_{m,max}(\delta_{m,f}-\delta_{m,0})} \tag{6}$$

Where $\delta_{m,max}$ means the maximum fracture separation displacement that can be given as

$$\delta_{m,max}=\max\left\{\min\left\{\delta_{m,max},\delta_{m,f}\right\},\delta_{m,0}\right\} \tag{7}$$

When $\delta_{m,max}\leqslant\delta_{m,0}$, adhesive is in a linear elastic status. According to Eq. (6-7), $\delta_{m,max}=\delta_{m,0}$ which indicates D=0 and traction-separation characteristics can be written as

$$\sigma_i=K\delta_i\quad(i=\mathrm{n,t,c}) \tag{8}$$

When $\delta_{m,0}<\delta_{m,max}<\delta_{m,f}$, adhesive is in damage evolutional stage. According to Eq. (6-7), $0<D<1$ and D outskirts to 1 with the increase of $\delta_{m,max}$, considering the interface may be in compression, traction-separation characteristics can be described as

$$\begin{aligned}\sigma_n&=\left(1-D+\frac{\langle-\delta_n\rangle}{-\delta_n}D\right)K\delta_n\\ \sigma_t&=(1-D)K\delta_t\\ \sigma_c&=(1-D)K\delta_c\end{aligned} \tag{9}$$

When $\delta_{m,f}\leqslant\delta_{m,max}$, adhesive invalids completely. According to Eq. (6-7), $\delta_{m,max}=\delta_{m,f}$ that means D=1 and the element occurs fracture, traction-separation characteristics is represented as

$$
\begin{aligned}
&\sigma_{n}=\frac{\left\langle -\delta_{n}\right\rangle}{-\delta_{n}}K\delta_{n}\\
&\sigma_{t}=\mu\sigma_{n}\\
&\sigma_{c}=\mu\sigma_{n}
\end{aligned}
\tag{10}
$$

where μ represents frictional coefficient between both sides of crack.

2.1.2 Model parameters of adhesive under wide temperature range

Mechanical parameters of adhesive contain initial stiffness, fracture strength and maximum energy release rate. The mechanical parameters of mode-I, mode-II crack are measured by means of Double Cantilever Beam test (see Fig. 3(a)) and End-Notch Flexure test (see Fig. 3(b))[27]. While the mode-III crack, caused by shear stress, is difficult to measure by experiments due to verticality between the shear stress direction and the extending direction of crack. So it is assumed that mode-II and mode-III share the same initial stiffness, fracture strength and maximum energy release rate in numerical simulation[28].

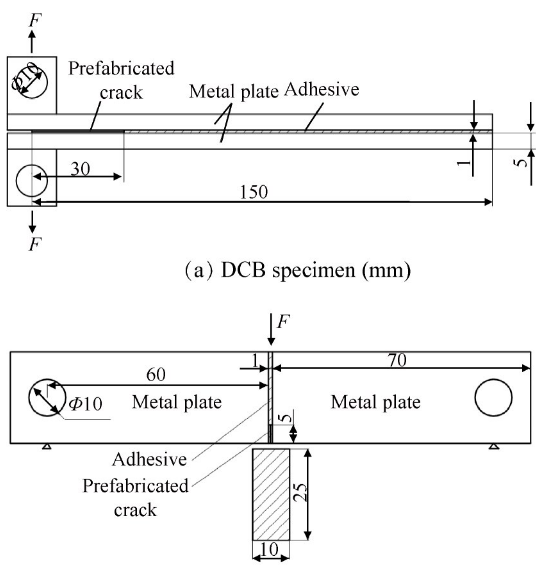

(a) DCB specimen (mm)

(b) ENF specimen (mm)

Fig. 3 Mechanical tests of adhesive

The parameters of cohesive zone model under wide temperature range were promoted according to Jia[29] and Walader[30]. Jia has considered with large displacement, end block effects[31] and round of crack tip[32] in experiments and obtained that all parameters of mode-I dropped with temperature from −40℃ to 50℃. Walader's results suggested that all parameters, except the mode-I maximum energy release rate, decrease with an increasing temperature in both loading modes in the temperature range from −30℃ to 80℃. Considering the difference of adhesive, this paper supposed that all parameters of adhesive used in flexible joint show a similar decline as the same slope as Jia during −55℃ ~ 65℃. Combined with the parameters at normal temperature[33-35], all the parameters under wide temperature range were obtained (see Table 1).

Table 1 Mechanical parameters of adhesive under wide temperature range

Temperature/℃	Fractrue strength/MPa			Maximum energy release rate /(N/mm)			BK coefficient
	σ_n	σ_t	σ_c	G_{IC}	G_{IIC}	G_{IIIC}	η
−55	39	56	56	0.37	0.68	0.68	1.5
−40	32	48	48	0.34	0.65	0.65	1.5
0	23	38	38	0.25	0.57	0.57	1.5
20	20	35	35	0.2	0.525	0.525	1.5
65	16	30	30	0.08	0.4	0.4	1.5

2.2 Sealing reliability model of flexible joint

2.2.1 Definition of sealing status of flexible joint

The sealing property is influenced obviously by the interfacial damage. The sealing status of interfacial elements are delimited according to damage parameter D_{ij} acquired in simulation results (see Table 2). The parameter $D_{ij}<0.95$ suggests that the element is not fracture and can keep sealing. When $D_{ij}\geq 0.95$, it implies that the element is fracture and can't provide adhesion, which means leakage when stretching. The theory of fluid pressure penetration, leakage occurred when the compressive stress (σ_c) is less than the vessel pressure (σ_v) and maintaining sealing when the compressive stress is larger than the vessel pressure, is considered when element is fracture and in compression. Fracture parameter f_{ij} is defined to describe the adhesion that $f_{ij}=1$ indicates leakage while $0\leq f_{ij}<1$ means sealing.

According to sealing status of interfacial elements, the sealing status of interface and flexible joint are defined in Table 3. Any column of elements on the interface leaks will result in leakage of interface but other conditions are not. And any interface leaks will lead to leakage of flexible joint.

Table 2 Sealing status of interfacial elements

Status of interfacial elements			Status	f_{ij}
Fracture	Stretching		Leakage	1
Fracture	Compression	$\sigma_c<\sigma_v$	Leakage	1
Fracture	Compression	$\sigma_c\geqslant\sigma_v$	Sealing	0
No fracture			Sealing	D_{ij}

Table 3 Sealing status of interface and flexible joint

Status	Interface	Flexible joint
Leakage of any row of elements	Leakage	—
Other cases	Sealing	—
Leakage of any interface	—	Leakage
Sealing of all interfaces	—	Sealing

2.2.2 Sealing reliability model

According to the theory of reliability, it is parallel relationship among any elements in a column and series relationship among any column of elements on the interface (see Fig. 4).

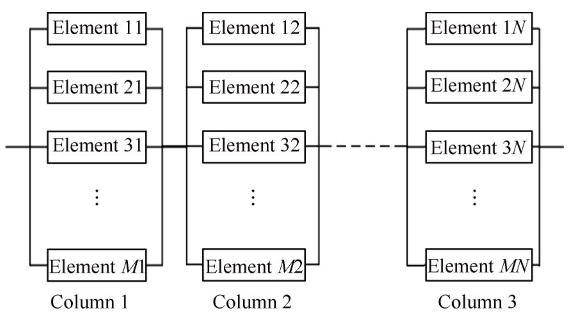

Fig. 4 Reliability diagram of mixed model

According to definition, the fracture probability of elements P_{ij} can be considered as fracture parameter f_{ij}

$$P_{ij}=f_{ij} \tag{11}$$

The reliability of elements can be described as

$$R_{ij}=1-P_{ij} \tag{12}$$

Because of parallel relationship among any elements in a column, reliability of column j can be given as

$$R_j=1-\prod_{i=1}^{M}(1-R_{ij}) \tag{13}$$

And due to series relationship among any column of elements, reliability of interface S is presented as

$$R_s=\prod_{j=1}^{N}R_j=\prod_{j=1}^{N}\left[1-\prod_{i=1}^{M}\left(P_{ij}\right)\right] \tag{14}$$

At the same time, series relationship is considered among interfaces by reliability theory (see Fig. 5).

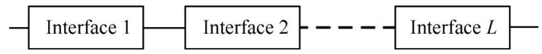

Fig. 5 Reliability diagram of series model

Therefore, the reliability of flexible joint with L interfaces is

$$R=\prod_{s=1}^{L}R_s \tag{15}$$

When the damage parameters D_{ij} of interfacial elements are little or even 0 in simulation result, suggesting the interface is almost no damage at all. In this case, the reliability calculated from Eq. (14) is 1, which is disagreement with decline of reliability after vectoring in fact. According to the analysis, Eq. (11) is revised by means of importance of elements in this paper.

The definition of importance of elements is that the elements in a layer have identical importance, the elements closer to vessel pressure are with a higher importance and the importance decreases exponentially with the increase of layers on the surface. Fig. 6 shows the importance analysis of flexible joint interfacial elements, the left is grid elements of interface and the right is importance–layers characteristics. For convenient description, rows from the closest to vessel pressure to another side are mark from 1 to i respectively. The shaded elements in a column all invalid will cause the interface invalid.

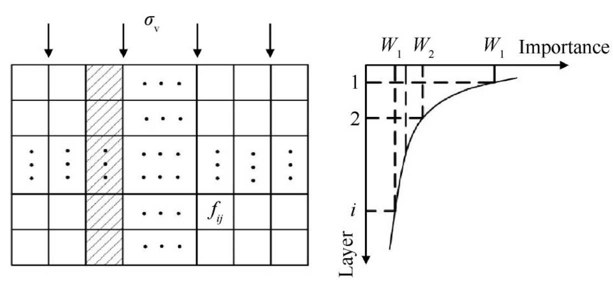

Fig. 6 Importance analysis of interfacial elements

According to the definition, the importance decrement function is presented as

$$W_i=e^{\frac{1-i}{n}} \tag{16}$$

where i is row number of elements, W_i is the importance of elements in row i, n is total number of rows. The fracture parameter of elements is distributed by importance decrement rule when $f_{ij}<f_0$ that the closer to ves-

sel pressure, the higher of fracture probability and importance, but the farther from vessel pressure, the lower of fracture probability and importance. Eq. (11) is revised as follows

$$P_{ij} = \begin{cases} f_{ij} & (f_{ij} \geq f_0) \\ f_0 W_i & (f_{ij} < f_0) \end{cases} \tag{17}$$

The determination of f_0 in Eq. (17) is that the interfacial sealing reliability of no damage interface is assumed as a constant value after vectoring, for example, 0.999 is selected in this paper. f_0, chosen from 0 to 1 for a set of constant importance values, is determined when the interfacial sealing reliability reaches the given value. In this paper, interfacial sealing reliability R_s=0.999 is selected and the corresponding f_0=0.588. Therefore, the revise of fracture probability of interfacial elements is accomplished by this method.

According to above analysis, the calculating flowchart of sealing reliability of flexible joint is illustrated (see Fig. 7).

2.3 FEA of flexible joint

2.3.1 Constitutive model of elastomer

The shear characteristics of elastomer made of butyl isoprene rubber are acquired by the quadruple shear test taking advantage of appropriate specimens under wide temperature range. Yeoh model is selected because of its ability to match experimental stress-strain data at small and large strain values as well as simulation results are in good agreement with experimental data[36]. The function of strain energy density E of the incompressible material described by Yeoh model is

$$E = \sum_{i=1}^{3} C_{i0} (I_1 - 3)^i \tag{18}$$

where C_{i0} are material parameters, I_1 is the first invariant of Green deformation tensor defined in terms of the elongation $\lambda_1, \lambda_2, \lambda_3$ given by

$$I_1 = \lambda_1^2 + \lambda_2^2 + \lambda_3^2 \tag{19}$$

The mechanical behavior of elastomer is affected by temperature dramatically under wide temperature range. The mechanical behavior decreases obviously with the rise of temperature and stress softening phenomenon is existed at a high temperature (see Fig. 8). Material parameters, fitted against the stress-strain data pairs measured from quadruple shear test by least square method, are shown in Table 4. Fig. 8 shows the predicated stress-strain curves by Eq. (18) compared with the test data.

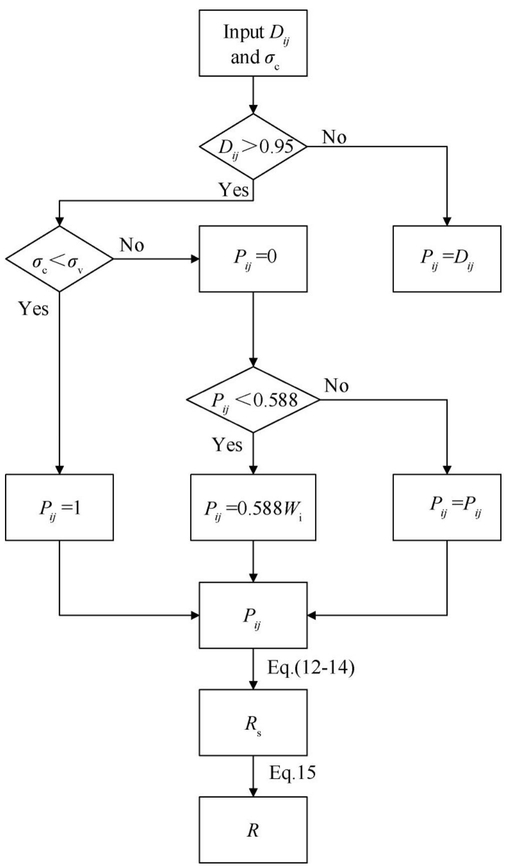

Fig. 7 Calculating flowchart of sealing reliability

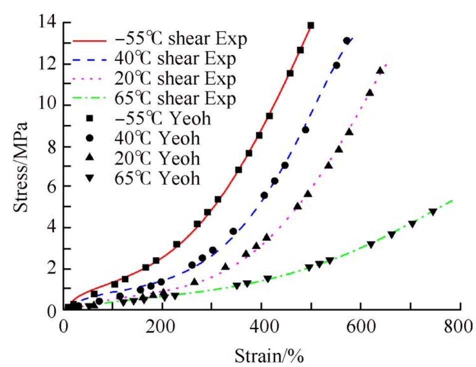

Fig. 8 Correlation of the Yeoh model with the test data at different temperature

Table 4 Yeoh model parameters under wide temperature range

Temperature/℃	C_{10}/MPa	C_{20}/MPa	C_{30}/MPa
−55	0.395007	2.1684×10^{-2}	-7.4886×10^{-5}
−40	0.186866	1.4192×10^{-2}	-7.4905×10^{-7}
20	0.110987	8.2972×10^{-3}	1.9761×10^{-5}
65	0.121561	1.6174×10^{-3}	1.6180×10^{-6}

2.3.2 FEA of flexible joint

The flexible joint is initially axisymmetrically shaped while non-axisymmetrically loaded (vectoring load), so 3D modeling is required. Considering the plane symmetry nature in the uniaxial vectoring circumstance, only one half of flexible joint is created. Fig. 9 shows the finite element computational mesh of flexible joint which composed of seven elastomers and six reinforcements as well as forward flange and after flange.

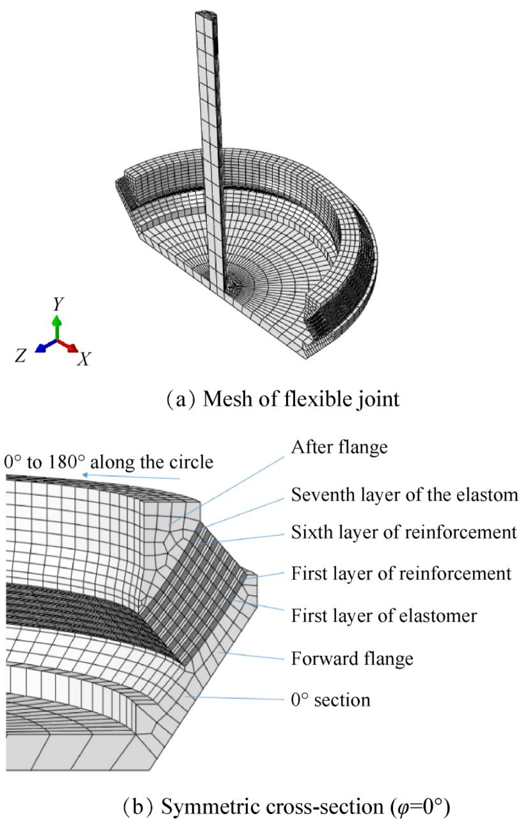

Fig. 9 Finite element model of the flexible joint

Elastomers are meshed with C3D8H and each elastomer is divided into 50×10×3 in the hoop, width and thickness direction respectively while reinforcements, forward flange and after flange which made of 30CrMnSiA steel are meshed with C3D8R and each reinforcement is divided into 50×10×2 in the hoop, width and thickness direction respectively, in ABAQUS (Version 6.14). The modulus of elasticity and Poisson's ratio of 30CrMnSiA steel are 205.8GPa and 0.3, respectively. The symmetry boundary condition ZSYMM is adopted on the symmetric cross sections (φ=0° and 180°) and Z direction displacement restrained. The after flange is fixed. All the outer wetted surface of the flexible joint model are subjected to the uniformly distributed vessel pressure. Angular displacement, $U_1=U_2=U_3=UR_1=UR_2=0$ and UR_3 is set as vectoring angle in ABAQUS, is applied to the pivot point that coupled with pendulum pole in order to represent the vectoring load.

3 Results and discussion

3.1 Effects of temperature on interfacial damage

In order to describe the interfacial damage, ratio of the amount of nodes in fracture areas to the total number of nodes on the interface is applied in this paper. Each interface is marked the number 1 ~ 14 from first elastomer to seventh elastomer, respectively.

Fig. 10 shows the damage contours of interface 14 at 4° vectoring angle under wide temperature range. The damage area appeared on one side of the interface at −55℃ ~ −40℃ but both sides above 0℃, and the number of damage elements increase drastically when the temperature up to 65℃. It suggests that the interfacial damage area increases with the rise of temperature.

Fig. 11 shows the damage of all interfaces increase with rise of temperature and rapidly at high temperature segment, which coincided with the result of contours. Also, the interface 14 has the maximum damage, interface 13, interface 1 and interface 2 drop gradually, and interface 3 ~ 12 have no damage almost under wide temperature range. The damage of interface 13 and 14 increase from 3% ~ 4% to 7% ~ 10% slowly with temperature rising, while interface 1 to 12 appear no damage nearly during −55℃ ~ 0℃. When the temperature is above 0℃, the damage of interface 1 and 2 increase obviously from 0% to 2% ~ 9%, at the same time, the damage of interface 13 and 14 raise from 7% ~ 10% to 12% ~ 20% with temperature.

Ostensibly, this phenomenon is related to the mechanical behavior of adhesive varying with temperature. It can be seen from Fig. 4 that fracture strength and critical energy release rate decrease monotonously as temperature rises, which indicates an easier interfacial damage will be occurred with a higher temperature. Essentially, this is relevant to microstructures of polymer adhesive. Macromolecular chains are frozen and only side polymer groups, branched chains as well as little chains can move under glass transition temperature. The deformation of adhesive is so much little that can hardly generate damage after loading due to minor changes of length and angle of bonds in frozen macromolecular chains. When the temperature exceeds glass transition temperature, the energy of molecular thermal motion is sufficient to surmount the barrier of inner rotating and macromolecular chains are excited to move by changing conformation of inner rotating single bond continuously. Therefore, large deformation emerges under little load which can cause damage easily.

3.2 Analysis of sealing reliability under wide temperature range

The importance decrement function is obtained as follows according to Eq. (16) because 10 elements are divided in the width direction and possessing eleven rows of nodes. The importance of each row is listed in Table 5.

$$W_i = e^{\frac{1-i}{11}} \tag{20}$$

Fig. 12 shows the interfacial sealing reliability of flexible joint under wide temperature range, combined with Fig. 11, it can be seen that sealing reliability and interfacial damage are inversely related. Interface 3 to 12 have the highest reliability 0.999, while interface 13 and 14 are the lowest. And the reliability of interface 1 and 2 reaches 0.999 below 0℃ while drops drastically with temperature rising above 0℃. The sealing reliability of interface 13 and 14 decrease rapidly with temperature during −40℃ ~ 20℃ while show a slow decline during −55℃ ~ −40℃ and 20℃ ~ 65℃. The reason is that the glass transition temperature of adhesive is in the

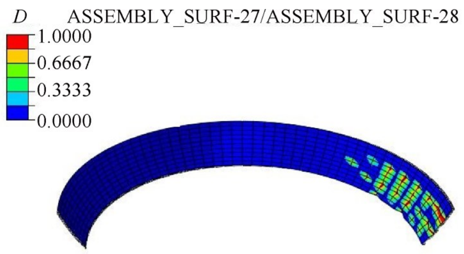

(a) T=−55℃

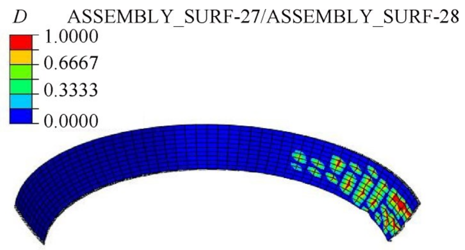

(b) T=−40℃

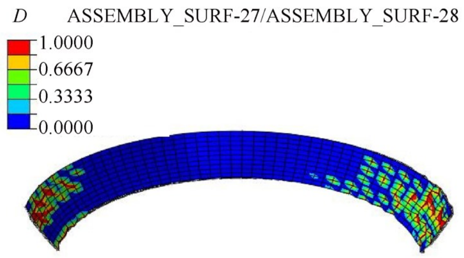

(c) T=0℃

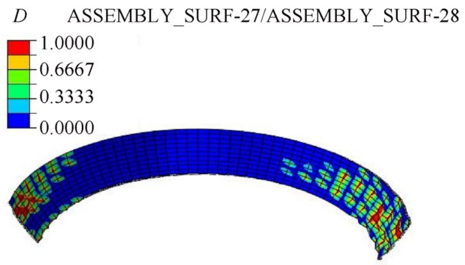

(d) T=20℃

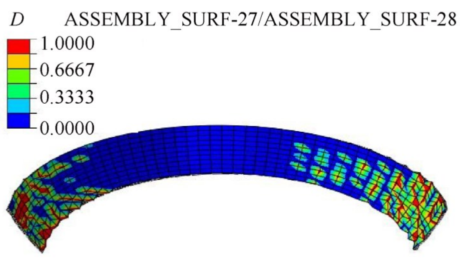

(e) T=65℃

Fig. 10 Damage contour of interface 14 at different temperature

Table 5 The importance of each row

i	1	2	3	4	5	6	7	8	9	10	11
W_i	1.0	0.913	0.834	0.761	0.695	0.635	0.580	0.529	0.483	0.441	0.403

range of −40℃ ~ 20℃ where the mechanical behavior of adhesive has a large diversification and instability, leading to serious increasing of interfacial damage, which is the decisive factor of apparent decline of interfacial sealing reliability.

The sealing reliability of flexible joint is calculated by Eq. (15). Fig. 13 presents the sealing reliability of flexible joint at 1MPa, 3MPa, 6MPa vessel pressure under wide temperature range. The sealing reliability of flexible joint drops rapidly during −55℃ ~ 20℃ while falling tendency slows down during 20℃ ~ 65℃. It is considered that adhesive presents a high elasticity like rubber when the temperature is above glass transition temperature. Though the number of fracture elements increases, a better contacting effect is generated among adhesive, elastomer and reinforcement that vessel pressure can't penetrate through out the fracture elements. Therefore, the falling tendency slows down during 20℃ ~ 65℃.

The pressure influence on the sealing reliability is illustrated in Fig.14. The reliability−temperature characteristics show that sealing reliability of flexible joint appears a downward tendency first and then increase with pressure, especially at high temperature. This phenomenon is consistent with engineering experience. The sealing reliability is high at a low pressure owing to little in-

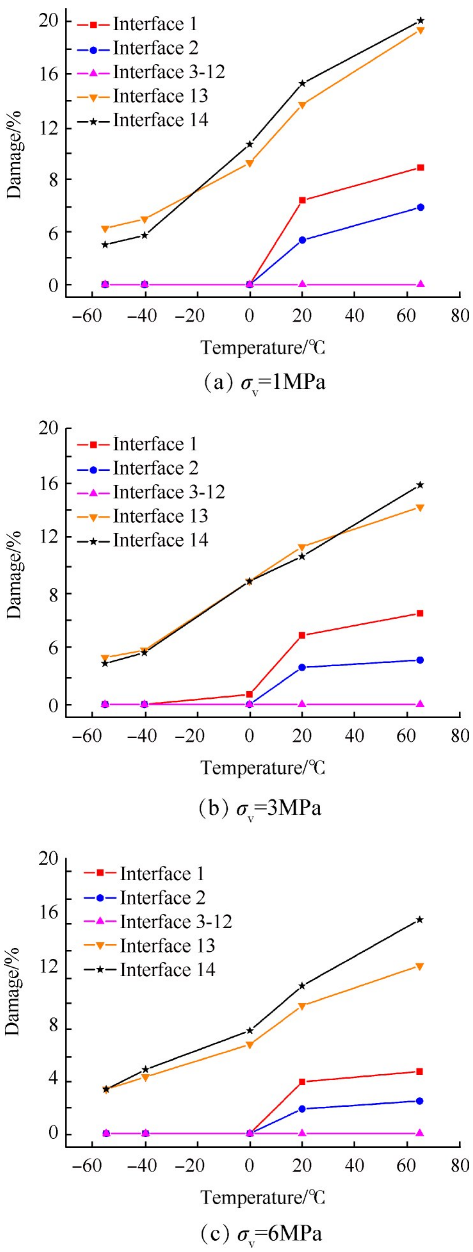

Fig. 11 Effects of temperature on damage of all interfaces

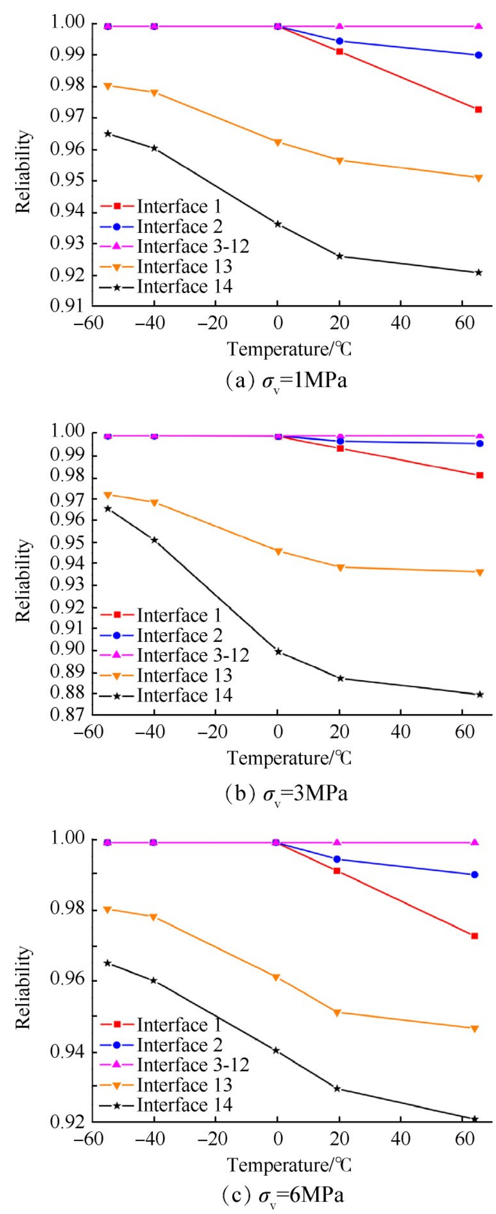

Fig. 12 Variation of interfacial sealing reliability with temperature at 4° vectoring angle

terfacial damage. Increasing pressure will cause two opposite effects. First, increasing pressure will lead to much interfacial damage which makes sealing reliability decrease. Secondly, the contact stress between elastomer and reinforcement rings increases with pressure that makes elastomer stick to reinforcement tightly. Therefore, the fracture nodes can still keep seal, which lets sealing reliability rise. According to Fig. 13, the second effect is more obvious at a higher pressure and temperature, this is the reason that sealing reliability declines first and then rises with pressure. In order to improve the sealing reliability of flexible joint, the working pressure is kept away from 3MPa and a high pressure will contribute to an excellent sealing reliability.

The sealing reliability is decided by the damage as well as the contact stress. The damage increases when the crack propagates, which reduces sealing reliability. However, the contact stress on the interface increases with vessel pressure, which contributes to improving sealing reliability. From Fig. 14, the increasing contact stress effect is more obvious than damage effect at a

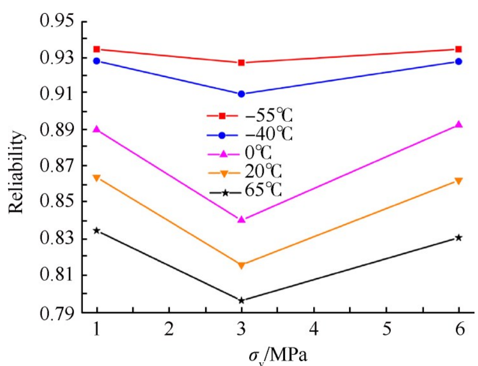

Fig. 14 Effects of vessel pressure on sealing reliability

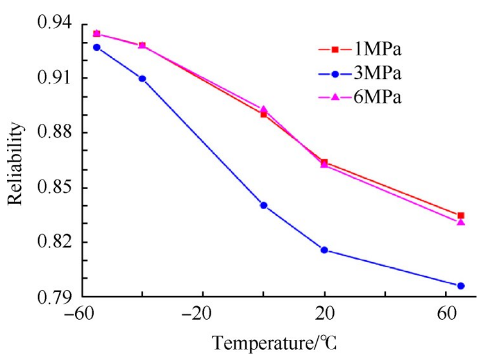

Fig. 13 Sealing reliability of flexible joint at different vessel pressure and 4° vectoring angle under wide temperature range

higher pressure. Therefore, the sealing reliability increases when the crack propagates at a high pressure.

4 Conclusion

The interfacial damage and sealing reliability of flexible joint have been analyzed under wide temperature range in this paper. The important summaries are listed below:

(1) Mechanical behavior of adhesive and butyl isoprene rubber both decrease with increasing temperature, meaning that fracture occurred easily at a high temperature.

(2) Sealing reliability and interfacial damage are inversely related. The interface bonded to the after flange has the maximum damage but the minimum sealing reliability, the damage of the penultimate interface, the interface bonded to forward flange as well as the second interface decrease gradually respectively and opposite of the sealing reliability, middle remaining interfaces have no damage almost and with the highest sealing reliability.

(3) Interfacial damage increases slowly first (3% ~ 4% at −55℃ and 7% ~ 10% at 0℃) and then grows rapidly (12% ~ 20% at 65℃) while sealing reliability of flexible joint declines linearly first (0.932 at −55℃ and 0.848 at 20℃) and then the falling tendency slows down (0.824 at 65℃). Sealing reliability of flexible joint is the highest at a low temperature under wide temperature range.

(4) Sealing reliability of flexible joint decreases first and then increases with pressure. The contact stress effect contributes to improving reliability while the damage effect is contrary, the contact pressure effect is more obvious at a higher pressure and temperature.

References:

[1] 阮崇智. 战术导弹固体发动机的关键技术问题[J]. 固体火箭技术, 2002, 25(2): 8-12.

[2] Robert F. H, Woodberry. Flexible Joints for Thrust Vector Control[R]. *AIAA* 75-1221.

[3] Bugrova A I, Bugrov G E, Bishaev A M, et al. Experimental Investigation of Thrust-Vector Deviation in a Plasma Thruster[J]. *Technical Physics Letters*, 2014, 40(2): 161-163.

[4] Olsen K E, Walsh J J, Thomas E L. Navy Terrier LEAP

Third-Stage Propulsion[C]. *Monterey*: *AIAA Missile Science Conference*, 1994.

[5] Uhrig G, Roussille C. Design Drivers and Technologies for Solid Propulsion of Interceptors[C]. *Arcachon*: *1st AIAA International Conference on Missile Defense*, 2003.

[6] Caveny L H, Geisler R L, Ellis R A, et al. Solid Rocket Enabling Technologies and Milestones in the United States[J]. *Journal of Propulsion and Power*, 2003, 19: 1038-1066.

[7] Descamps C, Gautronneau E, Rousseau G, et al. P80 SRM Low Torque Flex-Seal Development, Thermal and Chemical Modeling of Molding Process[J]. *EDP Science*, 2013, 2009: 141-152.

[8] Boury D, Gautronneau M, Daurat, at al. P80 Nozzle Development & Qualification Synthesis[C]. *Hartford*: *44th AIAA/ASME/SAE/ASEE Joint Propulsion Conference & Exhibit*, 2008.

[9] REN Jun-xue, ZHANG Xiao-guang, YANG Jing-xian, et al. Structural Analysis and Testing of a Miniature Flexible Joint under Pressure and Vector Loading[J]. *Journal of Mechanicaal Science and Technology*, 2014, 28: 3637-3643.

[10] SU Hao, REN Jun-xue, XUE Mu-yao, et al. Influence of Pressure and Deflection Loads on the Critical Behavior of Flexible Joint[J]. *Composite Structures*, 2017, 180: 772-781.

[11] 曹翠微，陈伟民，蔡体敏，等. 固体火箭发动机柔性接头的结构分析[J]. 推进技术，2006，27(5)：450-454.（CAO Cui-wei, CHEN Wei-min, CAI Ti-min, et al. Structural Analysis on Solid Rocket Motor Flexible Joint[J]. *Journal of Propulsion and Technology*, 2006, 27(5): 450-454.）

[12] 王春光，史宏斌，王雪坤，等. 高压下喷管柔性接头摆动力矩数值分析[J]. 推进技术，2011，32(2)：202-206.（WANG Chun-guang, SHI Hong-bin, WANG Xue-kun, et al. Numerical Analysis of Deflection Torque of Flexible Joint with High Pressure[J]. *Journal of Propulsion and Technology*, 2011, 32(2): 202-206.）

[13] 黄朝晖，张 潇，刘伟凯. 基于弧长法对柔性接头高压下屈曲响应研究[J]. 导弹与航天运载技术，2017，4：102-106.

[14] 安春利，常新龙. 柔性接头弹性件超弹性本构参数拟合和低压摆动非线性有限元分析[J]. 固体火箭技术，2008，31(1)：79-83.

[15] 王周成，李 耿，陈 妮，等. 容压对柔性接头摆动密封可靠性的影响[J]. 固体火箭技术，2016，39(3)：337-341.

[16] Lucas F M da Silva, Adams R D. Measurement of the Mechanical Properties of Structural Adhesives in Tension and Shear Over a Wide Range of Temperature[J]. *Journal of Adhesive Science and Technology*, 2005, 19(2): 109-141.

[17] Caggiano A, Schicchi D S, Etse G, et al. Meso-Scale Response of Concrete under High Temperature Based on Coupled Thermo-Mechanical and Pore-Pressure Interface Modeling[J]. *Engineering Failure Analysis*, 2018, 85: 167-188.

[18] Vernier Clemence, Dressler Marc, Seebich Hans-Peter, et al. Reliability of a Dual-Curable Adhesive Bond[C]. *Germany*: *17th International Conference on Thermal, Mechanical and Multi-Physics Simulation and Experiments in Microelectronics and Microsysterms*, 2016.

[19] XU Yang-jian, ZHAO Shuai, JIN Guo-hui, et al. Explicit Dynamic Fracture Simulation of Two-Phase Materials Using a Novel Meso-Structure Modelling Approach [J]. *Composite Structures*, 2019, 208: 407-417.

[20] Yang Q D, Thouless M D, Ward S M. Elastic-Plastic Mode-II Fracture of Adhesive Joint[J]. *International Journal of Solids and Structures*, 2001, 38(19): 3251-3262.

[21] Khoramishad H, Crocombe A D, Katnam K B, et al. Predicting Fatigue Damage in Adhesively Bonded Joints Using a Cohesive Zone Model[J]. *International Journal of Fatigue*, 2010, 32(7): 1146-1158.

[22] Dugdale D S. Yielding of Steel Sheets Containing Slits [J]. *Journal of Mechanical Physics and Solids*, 1960, 8 (2): 100-108.

[23] Barenblatt G I. The Mathematical Theory of Equilibrium Cracks in Brittle Fracture[J]. *Advances in Applied Mechanics*, 1962, 7: 55-125.

[24] Benzeggagh M L, Kenane M. Measurement of Mixed-Mode Melamination Fracture Toughness of Unidirectional Glass/Epoxy Composites with Mixed-Mode Bending Apparatus[J]. *Composite Science and Technology*, 1996, 56: 439-449.

[25] De Moura M, Goncalves J P M. Cohesive and Continuum Mixed-Mode Damage Models Applied to the Simulation of the Mechanical Behavior of Bonded Joints[J]. *International Journal of Adhesion and Adhesive*, 2008, 28(8): 419-426.

[26] Yang Q D, Thouless M D. Mixed-Mode Fracture Analysis of Plastically-Deformation Adhesive Joints[J]. *International Journal of Fracture*, 2001, 110(2): 175-187.

[27] Floros I, Tserpes K. Fatigue Crack Growth Characteriza-

tion in Adhesive CFRP Joint[J]. *Composite Structures*, 2019, 207: 531-536.

[28] HONG Yang, YAN Ying, TIAN Zi-yang, et al. Mechanical Behavior Analysis of 3D Braided Composite Joint Via Experiment and Multiscale Finite Element Method[J]. *Composite Structures*, 2019, 208: 200-212.

[29] 贾 登，郑 健，陈 雄，等. 三元乙丙橡胶薄膜黏接界面温度相关性力学性能[J]. 航空动力学报，2016，31(11)：2809-2816.

[30] Tomas Walader, Anders Biel, Ulf Stigh. Temperature Dependence of Cohesive Laws for an Epoxy Adhesive in-Mode I and Mode II Loading[J]. *International Journal of Fracture*, 2013, 183: 203-221.

[31] Williams J G. Large Displacement and End Block Effects in the "DCB" Interlaminar Test in Modes: I and II[J]. *Journal of Composite Material*, 1987, 21(4): 330-347.

[32] Blackman B, Kinloch A, Paraschi M, et al. Measuring the Mode I Adhesive Fracture Energy GIC of Structural Adhesive Joints: the Results of an International Round-Robin[J]. *International Journal of Adhesion and Adhesive*, 2003, 23(4): 293-305.

[33] 乔 玉，周光明，刘伟先，等. 复合材料阶梯形胶接接头渐进损伤分析[J]. 南京航空航天大学学报，2014，46(4)：632-637.

[34] Chandrathilaka E R K, Gamage J C P H, Fawzia S. Mechanical Characterization of CFRP/Steel Bond Cured and Tested at Elevated Temperature[J]. *Composite Structures*, 2019, 207: 471-477.

[35] De Moura M, Goncalves J P M. Cohesive and Continuum Mixed-Mode Damage Models Applied to the Simulation of the Mechanical Behavior of Bonded Joints[J]. *International Journal of Adhesion and Adhesive*, 2008, 28(8): 419-426.

[36] Shahzad M, Kamran A, Siddiqui M Z, et al. Mechanical Characterization and FE Modeling of a Hyperelastic Material[J]. *Journal of Materials*, 2015, 18(5): 918-924.

（编辑：刘萝威）